11th U. S. National Combustion Meeting
Organized by the Western States Section of the Combustion Institute
March 24-27, 2019
Pasadena, California

Effect of a Diffuser on Conditioning Flow Field Fluctuations at the Exit of a Rotating Detonation Combustor

J. Tobias, D. Depperschmidt, R. Miller, M. Uddi, A.K. Agrawal

Department of Mechanical Engineering, University of Alabama, Tuscaloosa, AL, USA; aagrawal@eng.ua.edu

Abstract: Pressure gain combustion (PGC) seeks to convert fuel's chemical energy simultaneously into thermal energy and mechanical energy, thereby reducing the entropy production in the process. Recent research has shown that the rotating detonation combustion or combustor (RDC) can provide excellent specific thrust, specific impulse, and large pressure gain through rapid energy release by continuous detonation in the circumferential direction. In this study, we present experimental results from RDC operated on methane and oxygen-enriched air to represent reactants used in gas turbines for land-based power generation. A thorough understanding of the velocity flow field exiting the combustor is important to develop future rotating detonation engine (RDE) designs, as well as to successfully implement the flow conditioning devices to power generating turbine hardware located downstream. The RDC is operated at high pressures in two ways through this study: 1) placing a back-pressure plate (BPP) downstream of the annular combustor, and 2) placing a diffuser downstream of the annular combustor. Time-resolved particle image velocimetry (TR-PIV) is applied at a frame rate of 50 kHz to quantify the RDC exit flow. A qualitative analysis is presented with vector data obtain from experimental testing. Results show that for the BPP configuration the highly periodic exit flow tilts in the azimuthal direction, indicating a significant circumferential velocity component. For the diffuser configuration the flow is dominantly axial, with an insignificant circumferential velocity component. The flow field undergoes cyclic fluctuations with the BPP, but not so with the diffuser. Results also show the challenges associated with achieving uniform seed distribution in this highly transient and rapidly changing flow field.

Keywords: Pressure Gain Combustion, Rotating Detonation Combustion, Particle Image Velocimetry

1. Introduction

Pressure gain combustion (PGC) has gained attention in the last decade for its potential to increase the fuel efficiency. This is realized by means of converting a portion of fuels' chemical energy directly into work by utilizing a detonation combustion process, and thus, reducing the entropy production [1-3]. Extensive research is ongoing to replace the deflagration combustor with a detonation combustion system in constant pressure, continuous flow systems, such as gas turbines [4]. Pulse Detonation Combustion (PDC) has been proposed as a solution, however challenges such as intermittent operation requiring sophisticated valve hardware with fast timing sequence, low operational frequencies, and inconsistent fuel-air mixing does not make PDC an immediately desirable solution in practice [5].

The rotating detonation combustor (RDC) uses the idea of a detonation wave propagating along a track, wherein the track is circular. This allows for the detonation wave to rotate continuously around an annulus as long as conditions remain favorable for detonation [6-7]. RDC hardware is known as rotating detonation engine (RDE), and the two terms are commonly used interchangeably. Figure 1 illustrates a simplified schematic of the RDC annulus during operation. Reactants at elevated pressures are fed into the bottom of the annulus via separate manifolds where mixing occurs post-injection via jets at the base of the annulus. The detonation wave then consumes the reactant mixture and propagates circumferentially as products exit the annulus axially and new reactants are introduced. As the detonation wave passes and reactions take place, the high-pressure and high-temperature products expand across an oblique shock wave attached to the moving detonation wave. Inlet pressures determine the power output of the RDC for a given fuel-air mixture, eliminating the need for complex valve mechanisms required in PDCs.

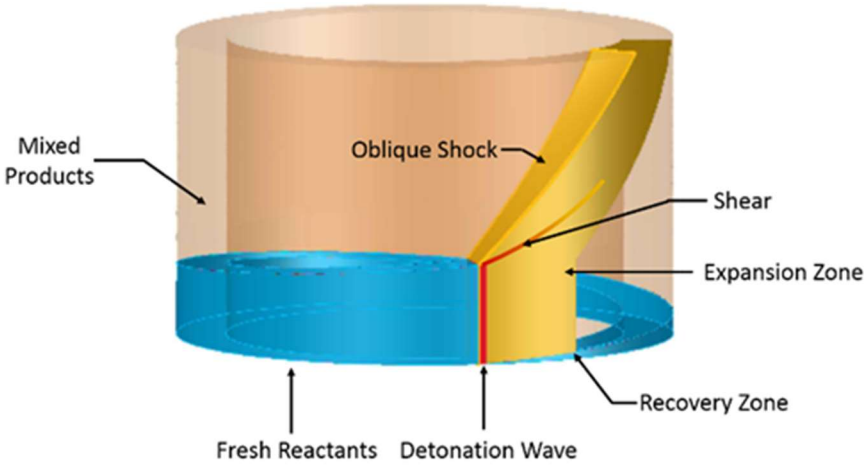

Figure 1. Simplified schematic of RDC wave.

The detonation wave speed is dependent on fuel and oxidizer selection, equivalence ratio, and reactant flow rate, among other parameters, and can exceed 2,000 m/s. At this speed, the thousands of rotations each second appear as a single combustion event, however upon high-speed investigation, the periodic nature of the detonation wave and subsequent oblique shock are revealed. It is common to experience a variety of modes regarding operation of an RDC including a single wave, multiple waves in one direction (co-rotating), and multiple waves in a counter rotation ("slapping") modes. Studies for RDC are increasingly focused on optical measurements to obtain quantifiable data of the detonation wave and the flow field in an effort to understand the important physical processes and to optimize designs for practical applications [8-11]. Detonation within the annulus has been optically studied using OH* Chemiluminescence carried out by Rankin et al. [12], as well as in the RDC exhaust flow by Tobias et al. [13]. Dynamic coupling between the detonation wave and the fuel plenum has also been studied by Fotia et al. [14].

Paxson [15] created a simplified 2D model of RDC with a coarse grid to reduce the computational cost while still achieving reasonable agreement with more complex simulations. Kailasanath and Schwer [16] used high fidelity 3D simulations to characterize the basic flow field associated with an RDE to identify the key parameters that affect the engine performance. They noted that the flow field exiting into a plenum from a RDE annulus without a center body or aerospike had small radial

velocities in addition to axial and azimuthal components of the flow. Nordeen et al. [17] modeled the RDE flow field, and compared the flow behavior through multiple configurations of attached flow conditioning devices. The non-axial flow component ("swirl") is detailed and shown to be in agreement with the conservation of momentum. They reported that the azimuthal flow fluctuations were effectively attenuated by a diffuser-like assembly including a converging-diverging (CD) nozzle.

Flow field measurements within the RDC would be particularly useful to the numerical simulation community, which has been eager for experimental data to conduct model validation. The present study is motivated by two significant objectives to advance the fundamental understanding of RDCs. First, the majority of the previous studies were inspired by RDC's potential for thrust augmentation realized by pressure gain. These studies have most commonly utilized hydrogen fuel. Currently, RDC technology is also being researched to replace the conventional combustion system in power generating gas turbines, and thus, methane is used as the fuel in this study. Second, the cyclic nature of rotating detonation results in large amplitude periodic pressure oscillations that must be attenuated after detonation, and if applied in practice, before entering a turbine. To complete this task a diffusor with a converging-diverging nozzle at the exit will be affixed to the end of the RDC annulus and evaluated using measurements by time-resolved particles image velocimetry (TR-PIV) technique.

2. Experimental Setup

The RDC in the Engine and Combustion Laboratory (ECL) at the University of Alabama is shown visually in Figure 2 and schematically in Figure 3. The modular design of the combustor, developed by Aerojet Rocketdyne, Inc. consists of three concentric spools and a circular center-body. The annular combustion chamber has an outer diameter of 10.0 cm, inside diameter of 8.0 cm, and height of 13.9 cm. The RDC annulus is positioned above an injector plate with discrete holes to introduce fuel and oxidizer into the combustor annulus through a circular manifold assembly. This study takes into account two different exit configurations: 1) a back-pressure plate (BPP) seen in Fig. 2a and Fig. 3a, and 2) a diffuser with an exit nozzle seen in Fig. 2b and Fig. 3b. Configuration 1 uses a BPP to simulate back-pressure that would be seen when coupled with a power generation gas turbine. This plate is secured above the top spool and consists of a converging-diverging (CD) nozzle. The throat area ratio across the BPP is 1.7. Configuration 2 involves a diffuser secured above the top spool of the RDC. The diffuser has a length of 23.5 cm and is terminated with a back-pressure CD nozzle with a throat area ratio of 2.0.

Operation of the RDC utilizes methane fuel and oxygen-enriched air as the oxidizer. Each reactant gas supply system (methane, air, and oxygen) consists of storage gas cylinder racks, sonic nozzles instrumented with pressure and temperature transducers to measure the mass flow rate, and an electro-pneumatic valve adjacent to the RDC to quickly turn on/off the flow. Air and oxygen lines combine to form the oxidizer line, and subsequently fuel and oxidizer lines feed into the respective plenum chambers located at the base of the RDC. RDC operation is initialized by igniting a hydrogen-oxygen mixture in a separate pre-detonation line, and introducing the resultant detonation wave radially into the RDC. The RDC is oriented vertically within a Lexan enclosure, and the test cell is equipped with supply of ventilation and exhaust air to safely release the

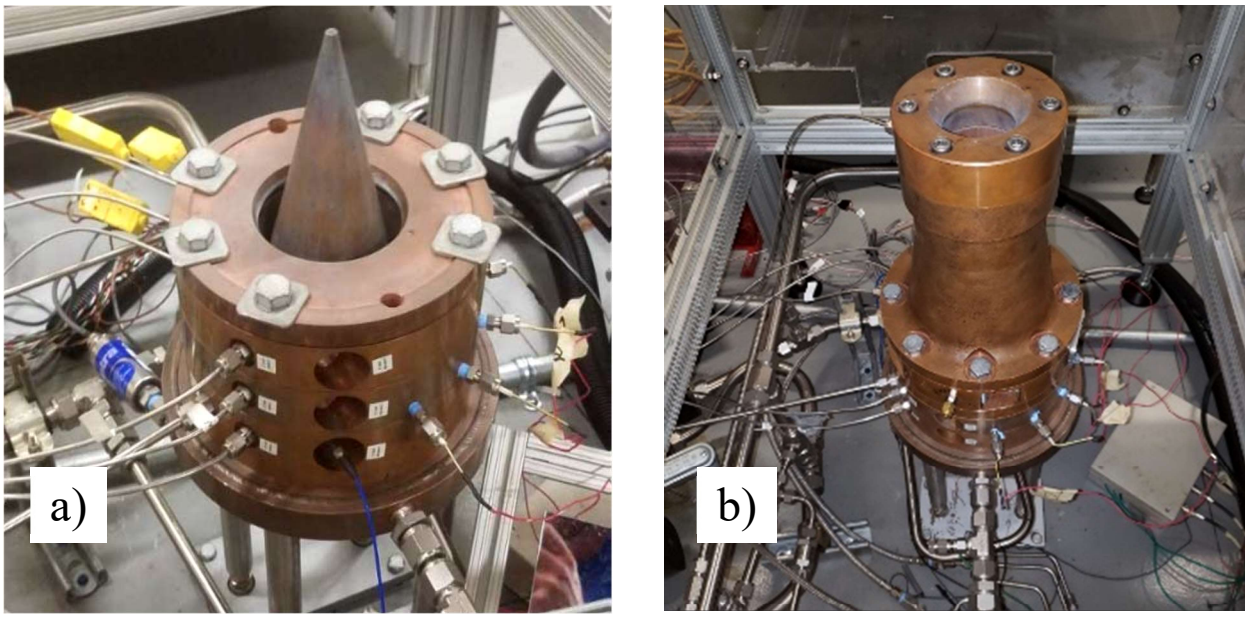

Figure 2. Photograph of RDE hardware: a) Back-Pressure Plate configuration, b) diffuser configuration

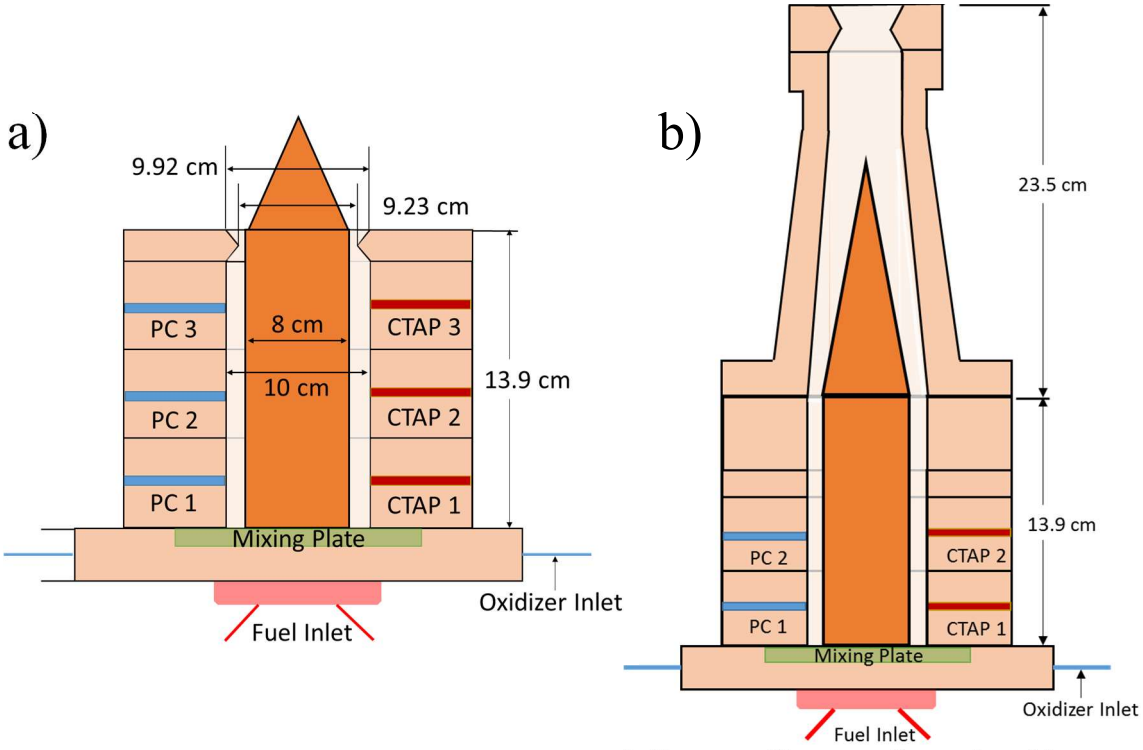

Figure 3. Schematic diagram of RDE hardware: a) Back-Pressure Plate configuration, b) diffuser configuration

combustion products to the atmosphere. The operation and timing of the experiment are precisely controlled by an in-house developed control system using multiple BeagleBone microprocessors to prevent deflagration combustion at the start of the experiment. Further details of the test facility, instrumentation, and operation are given in publications by Welch et al. [18] and Tobias et al. [13].

A Photonics, single-head, 35 W (0.35 mJ per pulse), 532 nm Nd-YAG laser is used for the time resolved - particle image velocimetry (TR-PIV). Figure 4a displays a diagram of the optical setup to create the laser sheet at the region of interest (ROI) in the flow field. The laser beam passes first through a spherical lens to optically focus the laser beam to maximize laser intensity at the ROI. The beam then passes through two cylindrical lenses to generate the laser sheet; a concave lens transforms the beam into a diverging laser sheet and a convex lens is used to collimate the laser sheet. This optical arrangement resulted in a laser sheet with minimal divergence angle and a sheet height similar to that of the field of view of the camera, both important factors to maximize the light intensity of the laser sheet. The sheet thickness (0.97 peak intensity thickness) at the region of interest is approximately 1 mm. Thus, only seed particles flowing with normal velocity greater than 1000 m/s could cross the laser sheet during the 1 μs time between the laser pulses. Such high flow velocities normal to the laser sheet are not expected, an assumption partly supported by the measurements. The region of interest (or camera field of view) is a square sheet 29.2 mm x 29.2 mm along a cord of the annulus in the middle of the annular gap. The difference between the two configurations was the adjustment of laser sheet height to account for the hardware length. Additionally, the laser offset from the center of the RDC is an offset distance determined by the total area of the opening at the nozzle exits for both configurations seen in Figure 4b and 4c.

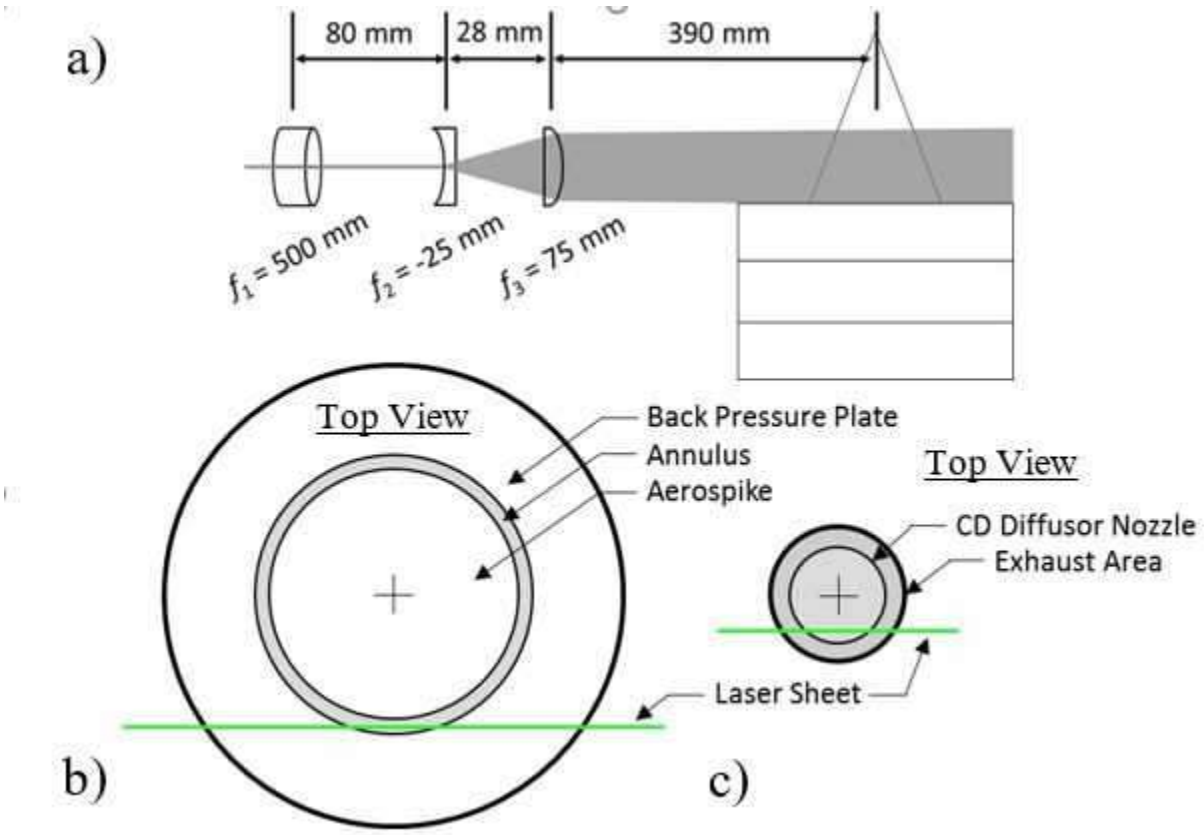

Figure 4. Schematic of the: a) optical system b) BPP configuration laser path across exit, c) diffuser configuration laser path across exit.

The present PIV system measures only two velocity components in an otherwise 3D flow field. We assume that the non-axial velocity component is purely circumferential, and it does not contain a radial component at the location of the region of interest. The flow field can therefore be discretized into axial and circumferential velocity components. Strictly, this assumption is valid only along the centerline of the field of view, i.e., x ≅ 12 mm where no net flow in the radial direction of the RDE is expected. However, away from the centerline of the field of view, contribution from the radial velocity component would be higher, and could affect the accuracy of the present circumferential velocity measurements.

A seeder system is used for this study in conjunction with the laser and high-speed camera for PIV imaging. The seeder operated on a separate air supply line, and the seeded airflow is injected into the main oxidizer flow line upstream of the RDE manifold. Several different seed particles were attempted previously, which led to the selection of 200 nm diameter ZrO_2 particles for the final experiments. This seed material was selected after careful consideration into a high pressure, oxygen-rich reacting environment. Additionally, the seeding system has undergone multiple design iterations aimed at improving seed distribution, and thus, obtain high quality TR-PIV images. Still, we suspect that pressure coupling from RDC operation can propagate upstream and prevent injection of seed flow at times during the test.

A high-speed camera, Photron SA5 Fastcam, is used to acquire the PIV images at acquisition rate of 100 kHz for a PIV acquisition rate of 50 kHz. A 532 nm band-pass optical filter was mounted in front of the camera lens to capture the light scattered from the seed particles within the laser sheet. The camera is positioned perpendicular to the ROI and 62 cm away from the laser sheet. The bottom edge of the laser sheet corresponds to y = 0 mm, and is aligned with the exit plane of the CD nozzle on the RDC or diffuser. An inspection window was cut into the protective Lexan blast shield enclosure to avoid distortion of PIV images by the intervening surfaces. Each PIV image is 256 x 232 pixels, which results in spatial resolution of 93.86 μm/pixel. Figure 5 presents the PIV timing diagram to synchronize the laser pulses with the PIV image capture sequence. For PIV acquisition rate of 50 kHz, a pair of PIV images was acquired at every 20 μs. The time between the two consecutive laser pulses (Δt) was set to 1.0 μs and was measured by an oscilloscope at 0.85 μs in pre-test with a 200 ns pulse width. This Δt was chosen after multiple trials to optimize the velocity resolution and image processing. The PIV timing sequence is implemented via a synchronizer controlled by the TSI Insight software. In addition, PIV image acquisition was initiated by the BeagleBone microprocessor system developed in-house and also controls all other flow and diagnostic components.

Insight 4G Data Acquisition, Analysis, and Display software from TSI was used to process the PIV images to calculate the velocity components. Due to the high velocity of the RDE exhaust flow, a starting interrogation window of 96 x 96 pixels and final interrogation window of 48x48 pixels were used with a double pass Recursive Nyquist grid. Computed velocity data was restricted to displacement of seed particles less than or equal to 30% of the starting spot interrogation window. The velocity flow field data set was then post processed, first via a local validation method consisting of a universal median test, in which velocity measurements are compared to the local median of the 3x3 interrogation neighborhood of the specific node. Variations of more than twice the circumferential or axial velocity measurement from this local median were discarded, and replaced by valid secondary peaks in the interrogation neighborhood when applicable. A

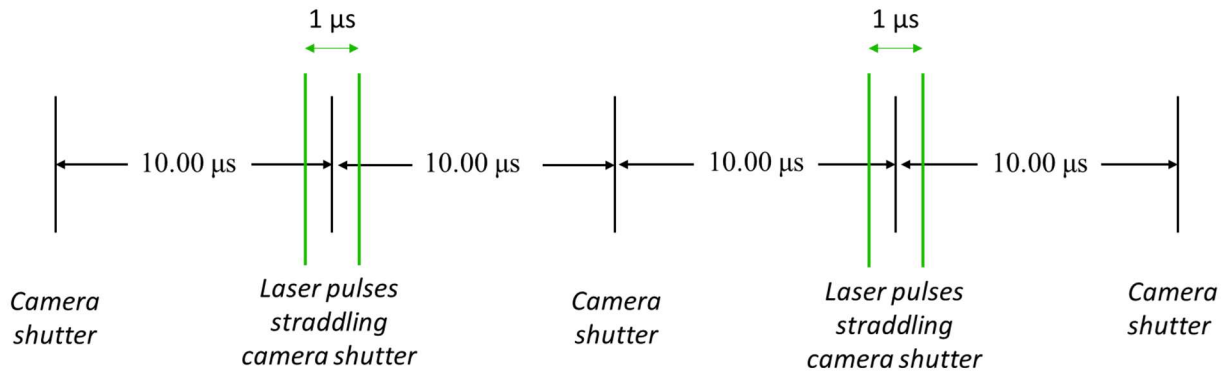

Figure 5. PIV timing diagram.

conditioning process was also applied in the post processing of the data in which holes in individual vector flow field matrices were filled using the 3x3 local median. This recursive filling technique was applied using measured vectors in the interrogation neighborhood, and the process was omitted if only previously analytically replaced vectors were present.

3. Results and Discussion

We have conducted over one hundred tests for various operating conditions, back pressure configurations, and optical and direct measurement techniques. Results presented in this study are primarily concerned with TR-PIV acquired flow fields at the exit of an RDC with: configuration 1 – a back-pressure plate (BPP), and configuration 2 – a diffuser. Tests were conducted with inlet flow rates of 0.0467 kg/s of methane, 0.161 kg/s of oxygen, and 0.1 kg/s of air, such that equivalence ratios were kept near stoichiometric conditions. OH* chemiluminescence, and high-speed video imaging measurements at a similar test point have been reported previously [13,18].

For each test case, one-thousand consecutive PIV image pairs (A and B) are obtained per run. Figure 6 shows a sample for three sets of these images; 1) a shock structure in BPP configuration which has just passed, 2) a region between the shockwave passages in BPP configuration, and 3) images at the exit from diffuser configuration. In each of these three image pairs, a disparity in brightness across A and B manifests from the upper half of the image in A to the lower half of the image in B. Upon close inspection, the structures in the bottom of frame B appear bright while a faint structure existed in frame A. The light intensity difference was caused by the single head laser system operated in dual mode pulsed at 0.852 µs to maximize the power output. In previous pre-test diagnostics, a photo-diode test has shown that although the first pulse has Gaussian intensity distribution, the second pulse has a more tailing effect.

Pre-processing techniques from the Insight software were used to decrease the difference in intensity, providing marginal success. The light disparity affects the vector quality in sections of the PIV images causing data processer to erroneously assign vectors in the negative axial direction. Although it is possible to have an occasional trivial negative axial vector in

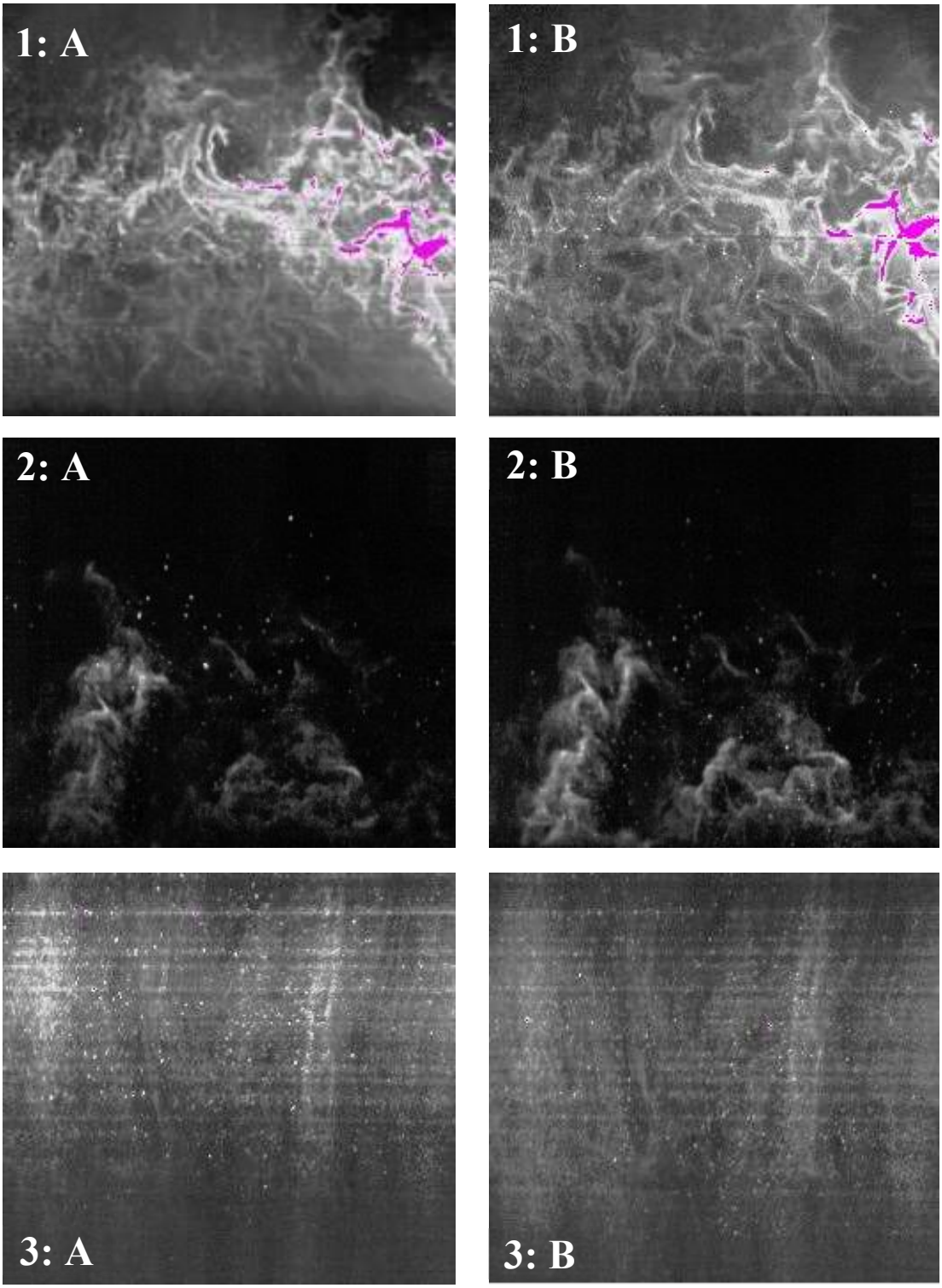

Figure 6. PIV images showing laser intensity disparity between image pairs A and B: 1) shock structure in BPP configuration, 2) region between shockwave passing in BPP configuration, 3) images at exit from diffuser configuration. Brightness variation can be seen from A to B, particularly in the bottom half of the frame for each set.

processing due to eddy structures, the vectors calculated from this light intensity disparity can be in the vicinity of -1000 m/s. For the BPP cases in Fig. 6, the quality of vectors varies through the cycle duration. The images with shock waves passing show regions of dense seed. This is likely caused by seed agglomeration near the shock wave due to its compressive effects. Images 1: A and B have purple local regions which represents regions of oversaturation of light intensity. Since 1: A has sufficient light intensity, the change of intensity in 1: B has little to no effect on vectors processed for images containing the detonation wave passing. Images 2: A and B have noticeably less seed than the 1: A and B making the change from 2: A to 2: B more likely to receive erroneous negative axial vectors. This was observed throughout the PIV image set for the BPP test. Again in the images for the diffuser case, 3: A and B, the light intensity changes from the upper half of the frame to the bottom half. Additionally, there is less clarity in these images which could be contributions from both a lack of dense seeding and potentially a much higher velocity than the BPP case. Light stratification can also be seen across the diffuser images, but the exact cause is unknown at this time. Resolving vector fields with the diffuser case proved difficult in processing, thus requiring manual post processing. Manual inspection of pixel displacements in diffuser images suggests that the axial velocity at the exit is very high, nearly 1500 m/s.

One indirect solution to avoid the intensity problem between frames is to create an algorithm to manually pre-process individual images to balance the intensity from frame to frame. This could be done through an external program before the images are loaded into the Insight processor. This is an area which will be considered for future work. A more direct solution is to use a dual head laser system which would allow for two high powered pulses without compromising performance.

The plots in Figure 7 show axial (top row) and circumferential (bottom row) velocities with the BPP configuration (left column) and the diffuser configuration (right column). Data in Fig. 7 pertain to a single spatial location, near the centerline, across all images; each image is 256 x 232 pixels (24 mm x 21.8 mm) and the point of interest is located near the middle of the frame at (12.4 mm, 3.2 mm). As stated previously, the PIV images were post-processed in the Insight software, though additional screening of vectors was conducted to meet further logical criteria. First, vectors with an absolute value less than 5 m/s in axial and circumferential velocities were omitted. Next, vectors with an axial velocity greater than 3,000 m/s were omitted as erroneous, as well as vectors with a significant negative axial velocity, particularly present for the diffuser case. Finally, vectors with circumferential velocities of greater than 2,000 m/s were also omitted. The remaining data are shown in Fig. 7. For the BPP configuration, 861 vector points remained after filtering and only 300 points remained for the diffuser case. Although, the small amount of adequate vectors makes quantitative analysis on the data set difficult, general trends can be observed and inspected to give insight for further testing.

First, the plot for the diffuser configuration shows a dense region of axial velocity data between 500 m/s and 1175 m/s, bounded by the light blue dashed lines. The same bound was transferred to the BPP configuration plot on the left. When considering points in this bounded region versus points outside: 45% of the total velocity data for the BPP configuration fall between the bounds, while 63% of the total velocity data for the diffuser configuration fall between the bounds. This is an expected trend, as the purpose of the diffuser design is to condition the flow to reduce the high amplitude flow fluctuations.

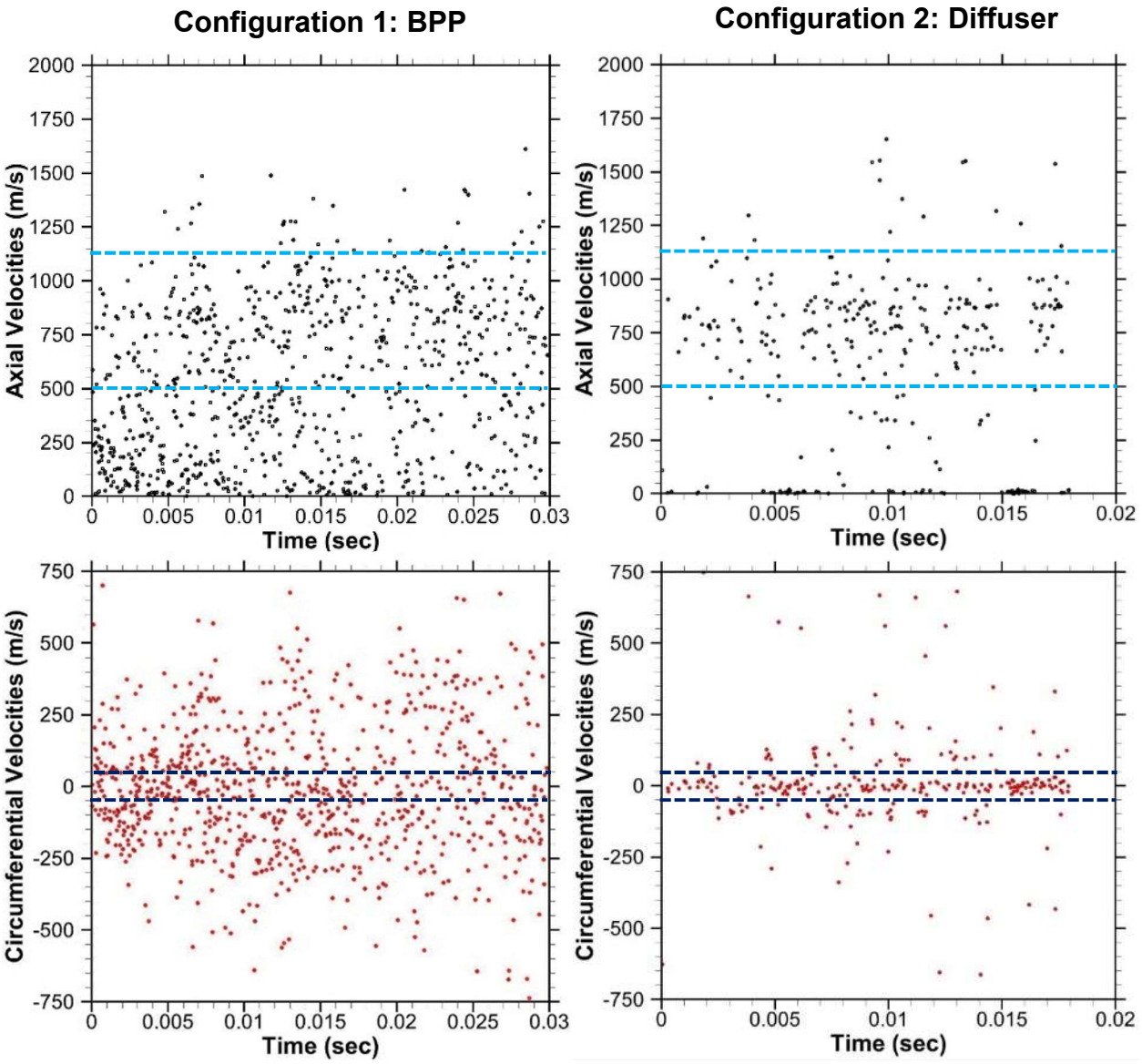

Figure 7. Plots of axial (top row) and circumferential (bottom row) velocities for 1) BBP (left column) and 2) Diffuser (right column). Light blue lines bound 500 m/s to 1175 m/s and navy blue lines bound ± 50 m/s.

Additionally, if attention is focused on the x-axis of the axial velocity plots, clusters of points are observed around every 5 ms, particularly evident for the diffuser configuration. The frequency of about 200 Hz is likely caused by the pressure coupling behavior as mentioned previously [14]. Furthermore, inspection of Fig. 7 shows that the circumferential velocity of the BPP configuration varies significantly compared to the diffuser configuration. Bounds were again applied, this time to ± 50 m/s, visualized as the navy blue dashed lines. For the BPP configuration, 20% of the all data point fall between the bounds, while 53% of the data points fall between the same bounds for the diffuser case. Again, this result supports the idea that the diffuser assembly is conditioning the flow to reduce the flow oscillation amplitude.

Next, Fig. 8 shows histogram axial and circumferential velocities for both cases. The histogram of axial velocity a significant percentage of data with near zero value for both cases. These are likely spurious data points caused by imperfect seed distribution and/or post processing since finite and reasonably high velocities are expected at the exit. For the BPP configuration, a larger amount of data scatter seen in Fig. 7 creates a dip in population at 500 m/s before increasing to 900 m/s, and then decreasing to lower velocities. Similarly, for the diffuser case, a large zero velocity population is seen in the axial velocity. However, histogram for high velocities has a much narrower distribution, indicating significant reduction in flow fluctuations by the diffuser. The results show that the diffuser is effective in reducing the axial flow fluctuations observed at the RDC exit.

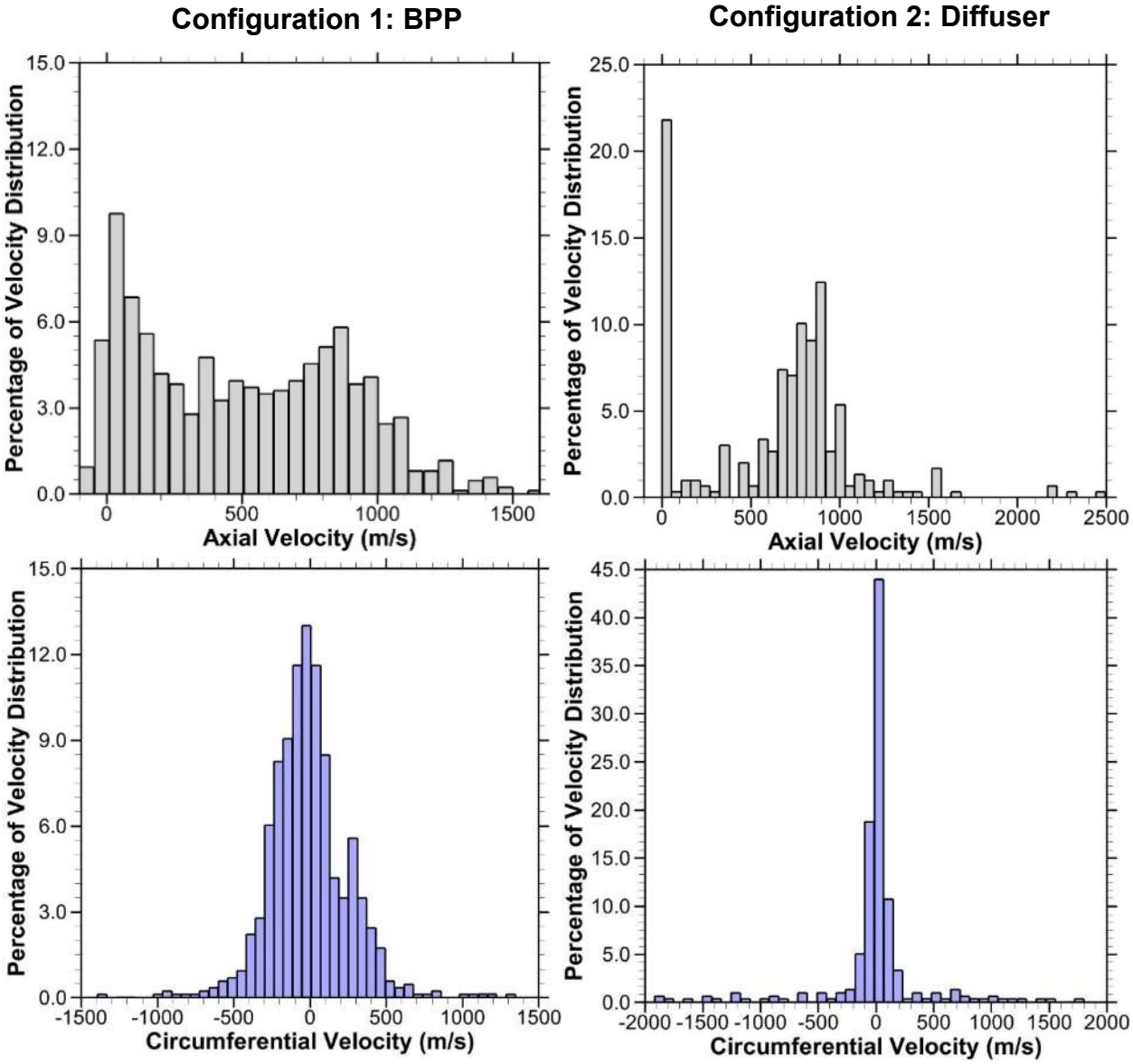

Figure 8. Histograms of axial (top row) and circumferential (bottom row) velocities for 1) BBP (left column) and 2) Diffuser (right column).

The circumferential velocity histograms in Fig.8 are centered around 0 m/s for both configurations. A Gaussian-like distribution is observed for the BPP configuration, with circumferential velocity changing direction and ranging in values from -500 m/s to 500 m/s. The change in the circumferential flow direction with the passing of the wave has also been reported in the numerical simulation of Nordeen et al. [17]. The histogram of the circumferential velocity at the diffuser exit shows a promising trend. Again, Gaussian distribution, albeit much sharper, is observed in this case, although analysis was limited in population size. Nearly half of the data points show near zero circumferential velocity, and nearly 80% of the data points range between -200 m/s and 200 m/s. Conversely, about 50% of the data points for the BPP configuration are within this velocity range. Note that velocity vectors which could not be recursively filled in PIV post-processing were assigned a zero total velocity, but any vector with a zero total velocity was eliminated for this analysis. The large percentage of nearly zero circumferential velocity data requires further assessment in the future. However, even with limited data, results indicate that the diffuser assembly is successfully conditioning the flow in the axial direction, and it is reducing flow fluctuations in both axial and circumferential directions. This is very encouraging, and indicates that flow oscillation generated in the RDC could be eliminated by the diffuser. However, in this case, velocity fluctuations still present with the diffuser, and indicate that further design improvements might be possible. Such design should however seek to minimize loss of pressure gain realized with the RDC.

Ideally, an analysis of the frequency domain would have also been considered, however limited data points made this problematic. Measurements showed that typical wave frequency measured by the PCBs and Ion Probes was 6,300 Hz for the BPP configuration. Visual inspection of the PIV images showed that for the BPP configuration, a wave passed the ROI for every eight images, indicating wave frequency of 6,250 Hz. It was not possible to conduct the same visual analysis with the diffuser configuration images, since a definitive wave structure could not be determined. However, there were multiple peaks between 6.5 kHz and 10 kHz from the RDC probes suggesting that multiple waves were present in the annulus. A process to determine the mode of multiple wave operation (counter-rotating versus co-rotating) is currently being developed to further analyze the results.

4. Conclusions

This study details initial experiments conducted in an RDC operated at a high pressure with methane fuel. The flow field at the exit of the RDC was measured by time resolved – particle image velocimetry (TR-PIV) operated at 50 kHz for: 1) a back-pressure plate (BPP) configuration, and 2) a diffuser configuration with an exit nozzle. Although the amount of useable data made it difficult to perform detailed analysis, results offered valuable insight into the RDC flow field. The study resulted in the following conclusions:

- Results demonstrate that the diffuser assembly conditions the flow to align it in the axial direction. The magnitude of peak circumferential velocity with the diffuser assembly is nearly half of that without the diffuser assembly.

- In both configurations, a sizable percentage of axial velocity values were nearly zero. This outcome is attributed to imperfect seed distribution, and/or PIV image quality. Further refinements are therefore possible.

- The flow exiting from the diffuser configuration shows streaks rather than individual particles some of the acquired PIV images. Thus, the axial velocities in this case could be much higher than expected because of the significant flow acceleration in the diverging section of the CD nozzle at the diffuser exit. Further tests should be conducted to assess how the time between laser pulses affects the accuracy of the measurements.

The TR-PIV diagnostics is challenging and requires further refinements to increase fidelity of acquired velocity data. Single pulse laser split into two pulses creates undesirable intensity various in the images that can be difficult to filter out. Thus, a laser system with dual diode heads should be used in future studies. The time between pulse must be precisely controlled, calibrated, and verified independently. Refinements to the pre-processing algorithm will increase the ability to remove spurious data from further consideration. Additionally, with longer data sets, quantitative analysis techniques such as cycle-to-cycle variations, frequency analysis, phase averaged cycle reconstruction, etc., can be implemented to gain further understanding into the effects flow conditioning devices on the RDC flow field.

5. Acknowledgments

This material is based upon work supported by the Department of Energy under Award Number(s) DE-FE0023983."

References

1. Zel’dovich, Yakov Borisovich. “Energy utilization of detonation combustion.” Zh. Tekh. Fiz., Vol. 10, No. 17, (1940): pp. 1455—1461.
2. Frolov, Sergey M., Aksenova, Victor, Guseva, P. A., Ivanova, Vladislav, Medvedeva,, S.N., and Shamshina, Igor. “Experimental Proof of the Energy Efficiency of the Zel’dovich Thermodynamic Cycle.” Physical Chemistry Vol. 459 Part 2 (2014): pp. 207-211.
3. Frolov, Sergey M., Aksenova, Victor, Ivanova, Vladislav. “Experimental proof of Zel’dovich cycle efficiency gain over cycle with constant pressure combustion for

hydrogen-oxygen fuel mixture", International Journal of Hydrogen Energy Vol. 40 (2015): pp. 6970-6975.

4. Sousa, Jorge, Paniagua, Guillermo, and Morata, Elena Collado. "Thermodynamic analysis of a gas turbine engine with a rotating detonation combustor." Applied Energy Vol. 195 (2017): pp. 247-256.
5. Roy, Gabriel D., Frolov, Sergey M., Borisov, Anatoli A., and Netzer, David W. "Pulse detonation Propulsion: Challenges, Current Status, and Future Perspective." Progress in Energy and Combustion Science Vol. 30, No. 6 (2004): pp. 545-672.
6. Voitsekhovskii, Bogdan Vyacheslavovich. "Stationary spin detonation," Sov. J. of Applied Mechanics and Technical Physics No. 3 (1960) pp. 157-164.
7. Nicholls, J. A., and Cullen, R. E. "The Feasibility of a Rotating Detonation Wave Rocket Motor," Univ. of Michigan, TR-RPL-TDR- 64-113, Ann Arbor, MI, 1964.
8. Lu, Frank K. and Braun, Eric M., "Rotating Detonation Wave Propulsion: Experimental Challenges, Modeling, and Engine Concepts." Journal of Propulsion and Power Vol. 30, No. 5 (2014) p. 1125-1142.
9. Wolanski, Piotr, "Detonative Propulsion." Proceedings of the Combustion Institute, Vol. 34, Issue 1 (2013): pp. 125-158.
10. Bykovski, F.A. and Zhdan, S.A., "Current Status of Research of Continuous Detonation in Fuel–Air Mixtures (Review)." Combustion, Explosion and Shock Waves Vol. 51, no.1 (2015) pp.21-35.
11. Kailasanath, Kazhikathra. "Recent Developments in the Research on Rotating-Detonation-Wave Engines." 55th AIAA Aerospace Sciences Meeting, AIAA 2017-07849-13, Grapevine, Texas, January 2017.
12. Rankin Brent A., Richardson Daniel R., Caswell Andrew W., Naples Andrew G., Hoke John L., Schauer Frederick R. "Chemiluminescence imaging of an optically accessible non-premixed rotating detonation engine", Combustion and Flame Vol. 176. (2016) 12-22.
13. Tobias, J., Depperschmidt, D., Miller, R., Uddi, Mruthunjaya, and Agrawal, Ajay K. "OH* Chemiluminescence Imaging of the Combustion Products from a Methane-Fueled Rotating Detonation Engine." Journal of Engineering for Gas Turbines and Power, Vol. 141, Issue 2 (2019).
14. Fotia Matthew L., Hoke, John L., and Schauer, Fred, "Propellant Plenum Dynamics in a Two-dimensional Rotating Detonation Experiment." 52nd AIAA Aerospace Sciences Meeting, AIAA Paper No. 2014-1013, National Harbor, Maryland, 13-17 January, 2014.
15. Paxson, D.E. "Numerical Analysis of a Rotating Detonation Engine in the Relative Reference Frame." 52nd AIAA Aerospace Sciences Meeting, AIAA 2014-0284, 2014.
16. Kailsanath, K. and Schwer, D.A. "High-Fidelity Simulations of Pressure-Gain Combustion Devices Based on Detonations." Journal of Propulsion and Power Vol. 33, No. 1, January-February 2017.
17. Nordeen, C., Schwer, D., Corrigan, A., and Cetegen, B. "Radial Effects on Rotating Detonation Engine Swirl." AIAA Propulsion and Energy Forum. AIAA 6.2015-3781, Orlando, FL, July 27-29, 2015.
18. Welch, Cooper, Depperschmidt, Daniel, Miller, Robert, Tobias, Jonathan, Uddi, Mruthunjaya, and Agrawal, Ajay K. "Experimental Analysis of Wave Propagation in Methane-Fueled Rotating Detonation Combustor," Proceedings of ASME Turbo Expo 2018, ASME Paper GT2018-77258, Oslo, Norway, June 11-15, 2018.